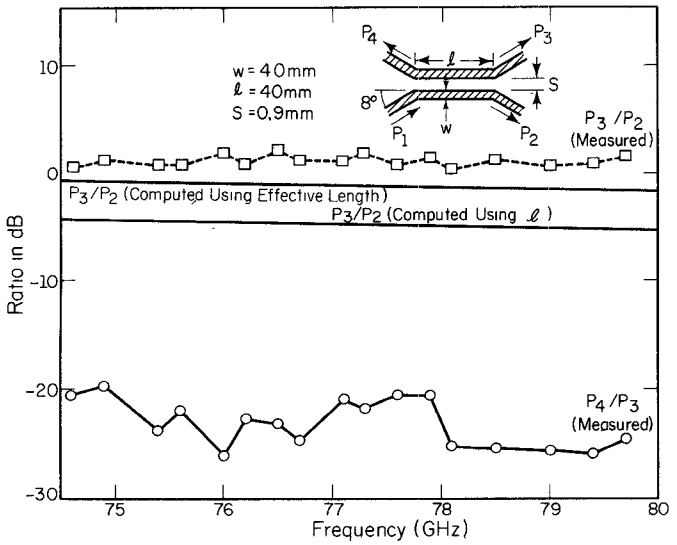

Fig. 7. Computed and measured performance of distributed directional coupler.

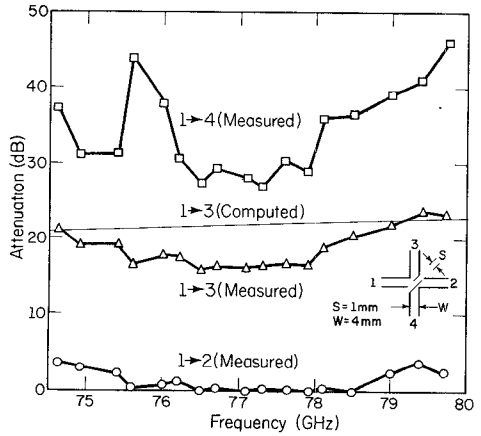

Fig. 8. Computed and measured performance of beam-splitter-type coupler.

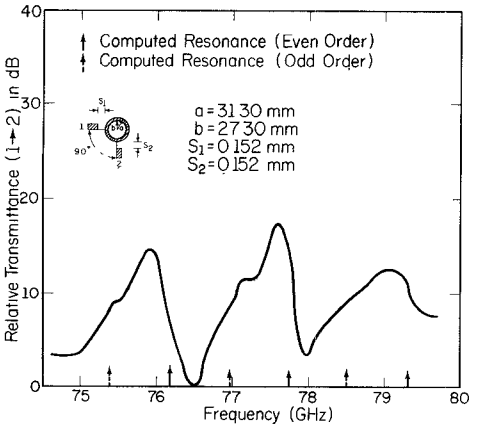

Fig. 9. Transmission characteristics of ring resonator.

frequencies, probably due to the strong coupling effects, while the odd-order resonances remain essentially unshifted. The location of the coupling arm 90° from the excitation arm places it at a null for odd-order resonances. This causes the weak response of the odd-order resonances as seen in the frequency characteristics of the ring resonator. Q of the resonator was found to be too low to be practical in its present form, mainly due to radiation associated with the curve. It is necessary to investigate and reduce the radiation phenomena by choice of material, structural parameters, etc.

VI. Conclusions

Several passive components for the IS millimeter-wave IC's have been described and analyzed. Results for theoretical as well as experimental studies were presented and reasonable agreement was observed. The salient design features for fabrication of these components have also been presented.

References

[1] M. V. Schneider, "Millimeter-wave integrated circuits," *IEEE MTT Symposium*, Boulder, CO, pp. 16–18, June 1973.
[2] P J. Meier, "Two new integrated-circuit media with special advantages at millimeter wavelengths," *IEEE MTT Symposium*, Chicago, IL, May 22–24, 1972.
[3] H. Jacobs and M. M. Crepta, "Electronic phase shifter for millimeter-wave semiconductor dielectric integrated circuits," *IEEE Trans. Microwave Theory Tech.*, vol. MTT-22, no. 4, pp. 411–417, April 1974.
[4] R. M. Knox and P. P. Toulios, "A V-band receiver using image line integrated circuits," *Proc. National Electronics Conf.*, vol. 27, pp. 489–492, Oct. 1974.
[5] T. Itoh, "Inverted strip dielectric waveguide for millimeter-wave integrated circuits," *IEEE Trans. Microwave Theory Tech. (Special Issue on Millimeter Waves, Circuits, Components, and Systems)*, vol. MTT-24, pp. 821–827, Nov. 1976.
[6] K. Kurokawa, *An Introduction to the Theory of Microwave Circuits*. New York: Academic Press, 1969.

Design, Implementation, and Performance Analysis of a Broad-Band V-Band Network Analyzer

L. T. YUAN, G. M. YAMAGUCHI, MEMBER, IEEE, AND J. E. RAUE, MEMBER, IEEE

***Abstract*—A novel V-band network analyzer has been developed for circuit and/or device characterization in the 55–65-GHz frequency range. Swept frequency techniques are utilized to simplify device design and network analysis over a wide range of operating frequencies. The design, fabrication, and performance of the unit is presented along with an error analysis for verification of measurement accuracies.**

Introduction

In recent years network analyzers have been used extensively for circuit and device characterization. They are powerful tools for optimizing circuit or device performance, particularly for broad-band applications where circuit or device parameters have to be known over a wide range of frequencies. However, commercial network analyzers currently available can only be operated up to *Ka*-band frequencies (26.5–40 GHz). For frequencies higher than *Ka* band, circuit and device characterization has to rely on the slotted line techniques by performing fixed-frequency point-by-point measurements. The fixed-frequency point-by-point measurements are not only tedious and time consuming, but also quite often fail to identify resonances between measurement points.

Increasing interest in communications systems operating at V-band frequencies (50–75 GHz) has created the need for the evaluation of circuits and devices at V-band frequencies. It is this demand that has prompted the development of a V-band network analyzer. This unit is capable of operation over a

Manuscript received May 20, 1976; revised July 23, 1976.
The authors are with the TRW Systems Group, Redondo Beach, CA 90278.

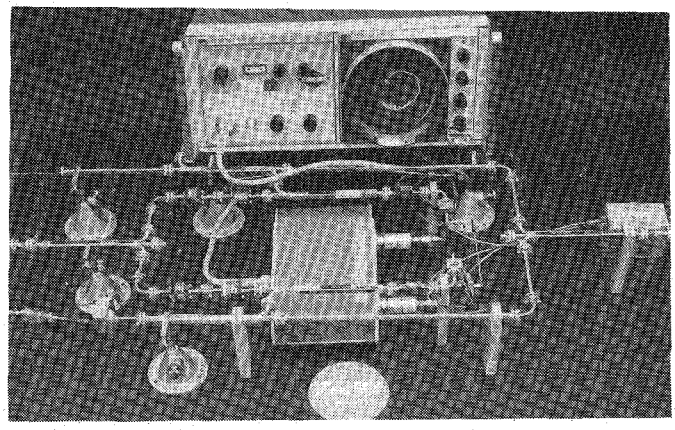

(a)

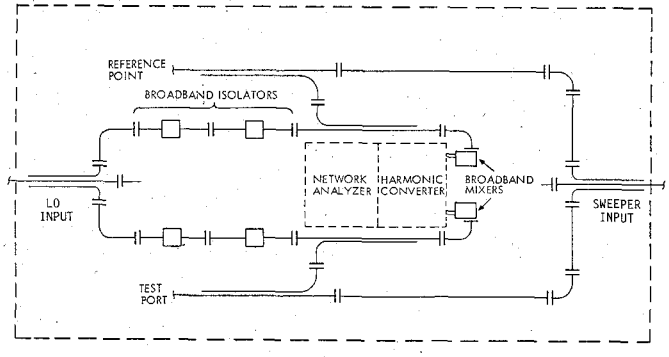

(b)

Fig. 1. V-band network analyzer. (a) Mechanical configuration. (b) Schematic diagram.

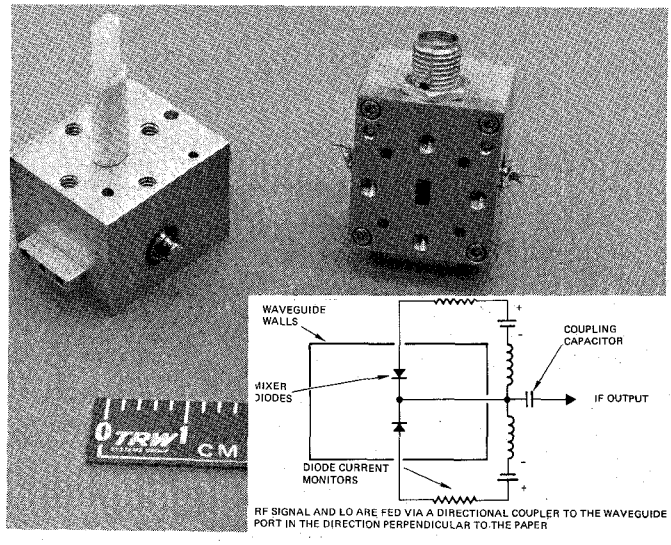

Fig. 2. V-band crossbar mixer.

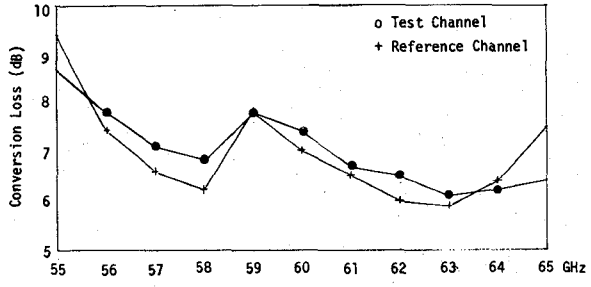

(a)

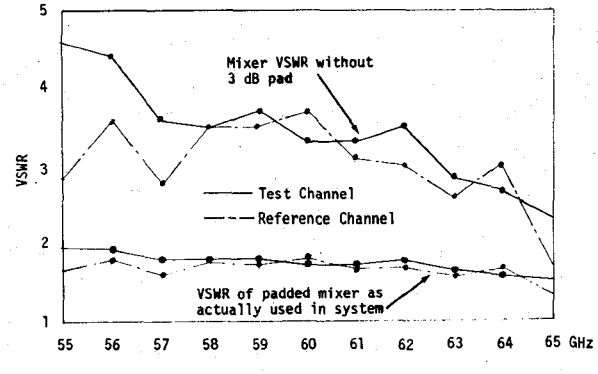

(b)

Fig. 3. (a) Conversion loss versus frequency of matched mixer pair. (b) VSWR versus frequency of matched mixer pair.

frequency range from 55 to 65 GHz. The broad-band performance of the present design results in a continuous measurement over a 10-GHz band with a single sweep. This substantially simplifies the measurement procedure since only a single reference short calibration is required, and measurements can be performed over the entire 10-GHz range without interruption.

System Description

The V-band network analyzer consists of a reflection test unit, a network analyzer (HP8410A), a harmonic converter (HP8411A), a 55–65-GHz sweep oscillator (Hitachi MS371/MM435), a high-Q avalanche diode oscillator, and a matched pair of reflectometers operated in parallel as shown by the mechanical configuration in Fig. 1(a). It is a symmetrical coplanar design which substantially simplifies hardware fabrication by eliminating complicated waveguide bends and minimizing waveguide lengths to reduce circuit losses. Fig. 1(b) shows the schematic diagram of the setup.

Broad-Band Mixer Design

The heart of the reflection test unit is a matched pair of broad-band mixers. These mixers, employing a crossbar configuration [1], [2], feature low conversion loss and broad-band performance. However, the accuracy of the V-band network analyzer depends on how well the two mixers can be matched in the microwave circuit design and, particularly, the tracking ability of the two mixers over the entire RF operating range.

The V-band mixer consists of a crossbar wafer mount, two Schottky-barrier diodes, and a backshort housing as shown in Fig. 2. The backshort housing also serves as a mounting block for the wafer mount. The crossbar diode wafer was fabricated with two back-to-back Schottky-barrier diodes connected in series across a metal crossbar. The opposite ends of the diodes are connected to the broad walls of the waveguide as shown schematically in the insert of Fig. 2. The RF signal and local oscillator power are fed to the waveguide port via a directional coupler. The IF output signal is extracted from the center crossbar via an OSM coaxial connector.

The performance of the crossbar mixers was excellent, particularly their RF and IF bandwidths which exceed the frequency response capability of the instrumentation used. Exceptionally broad IF bandwidth was achieved which covered a multioctave bandwidth from 2 to 12 GHz with VSWR less than 2:1. The extremely wide IF bandwidth of the mixer design has made

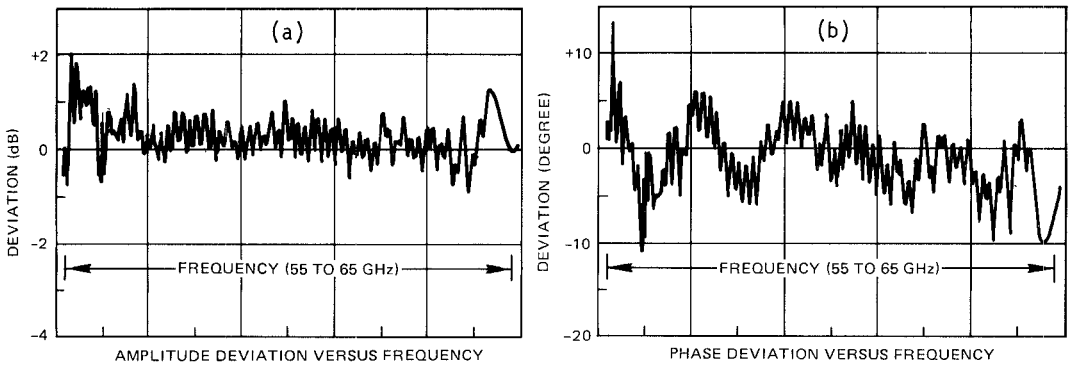

Fig. 4. Amplitude and phase deviation versus frequency.

possible the use of only a single sweep to perform the entire 10-GHz RF measurements. This eliminates the repetitive calibration procedure over every 2 GHz of the RF bandwidth as required for the commercial network analyzers. The conversion loss of the mixers was 4 and 4.5 dB, respectively, when measured at the best tuned frequency of 59 GHz. For broad-band tracking, the mixers were retuned in the system to obtain the best tracking over the entire 10-GHz frequency range. Fig. 3(a) shows the conversion loss of the mixers measured over the 10-GHz range. The loss differential between the two mixers was approximately ± 0.25 dB including the conversion, mismatch, and parasitic losses of the mixers, except for the end points at 55 and 65 GHz where the maximum deviation is about 1 dB. Fig. 3(b) shows the VSWR of the mixer measured in the system.

System Performance

The system performance of the V-band reflection test unit was evaluated by measuring 1) the overall system tracking, 2) the source reflection coefficients at both the test and the reference channels, and 3) the effective directivity of the system.

The overall system tracking ability was determined by measuring the amplitude and phase deviations. Fig. 4(a) and (b) shows the swept frequency response over the 55–65-GHz frequency range, when tested with the test port terminated by a fixed short circuit. The measured amplitude and phase deviations were ± 1.5 dB and $\pm 12°$, respectively. For a narrower band operation, i.e., 56–64 GHz, the amplitude and phase deviations were ± 1.1 dB and $\pm 8°$, respectively. The larger amplitude and phase deviations at the end points of 55 and 65 GHz are primarily due to higher loss differential of the mixers at these frequencies as shown in Fig. 3(a) and (b).

The source reflection coefficient at either the test or the reference channel, which is a measure of mismatches at the source, was measured by terminating the test port with an adjustable short circuit and the reference port by a fixed short circuit. The measured maximum source reflection coefficient over the 55–65-GHz range was 0.09.

The effective directivity of the system was measured by the sliding load technique [3]. The measured directivity over the 55–65-GHz range was greater than 35 dB, corresponding to a residual VSWR of 1.036:1 at the test port.

Design Considerations and Error Analysis

Meaningful swept frequency measurements place stringent requirements on the amplitude and phase tracking characteristics of all components in the system, particularly the broad-band mixer pair. The frequency response tracking of the matched mixer pair is critical for achieving accurate broad-band measurement capability. The use of low conversion loss mixers together with low-loss components is required to achieve wide dynamic range of the system design. This reduces noise contribution from the system, thereby making possible the measurement of small reflection coefficients.

The primary errors in measurements are associated with the source mismatch and the effective directivity of the reflectometer of the test unit. High effective directivity directional couplers are required for making high accuracy measurements as will be shown later in this section. The measurement of the effective directivity of a coupler includes the intrinsic directivity and a mated pair of flanges to the sliding load. In all waveguide systems, the mated flanges contribute to the measured directivity unless one places a sliding load element inside the coupler, thereby eliminating flange contributions. A directivity specification of this type is of no value to the design engineer since flange mismatches are very critical in millimeter-wave circuit characterization. Stable local oscillators and swept frequency sources are required for this unit to maintain phase lock of the network analyzer over the desired range. Initially, commercial solid-state frequency sources were used in the setup. However, a network analyzer phase lock could not be achieved due to excessive FM noise on the signal. Therefore, a cavity stabilized avalanche diode oscillator was developed for use as the local oscillator source, and a Hitachi BWO sweeper was used for the swept signal input.

The accuracy of the V-band reflection test unit is established by the directivity of the couplers, source mismatch, and calibration error of the system. The uncertainty in magnitude $\Delta\Gamma$ and phase Φ_e of the measured reflection coefficient is given as follows:

$$\Delta\Gamma = \pm(\Gamma_d + \Gamma_e\Gamma_L + \Gamma_s\Gamma_L^2), \quad [4], [5] \tag{1}$$

$$\Phi_e = \pm\sin^{-1}\left(\frac{\Delta\Gamma}{\Gamma_L}\right) \tag{2}$$

where

- Γ_d reflection coefficient corresponding to the value of directivity of the reflection test unit [4], [5];
- Γ_s source reflection coefficient at test port [4], [5];
- Γ_e calibration error due to a finite directivity and source mismatch, which results when the system is calibrated using only a fixed short as a reference and given by $\Gamma_d + \Gamma_s$ in a waveguide system [4], [5];
- Γ_L nominal value of the measured reflection coefficient.

(Note: The Γ_e term can essentially be removed in coaxial systems by using short circuit and an open circuit in the calibration technique. However, it is present in the waveguide system since a fixed short circuit is used as the reference for the measurement of phase and magnitude.)

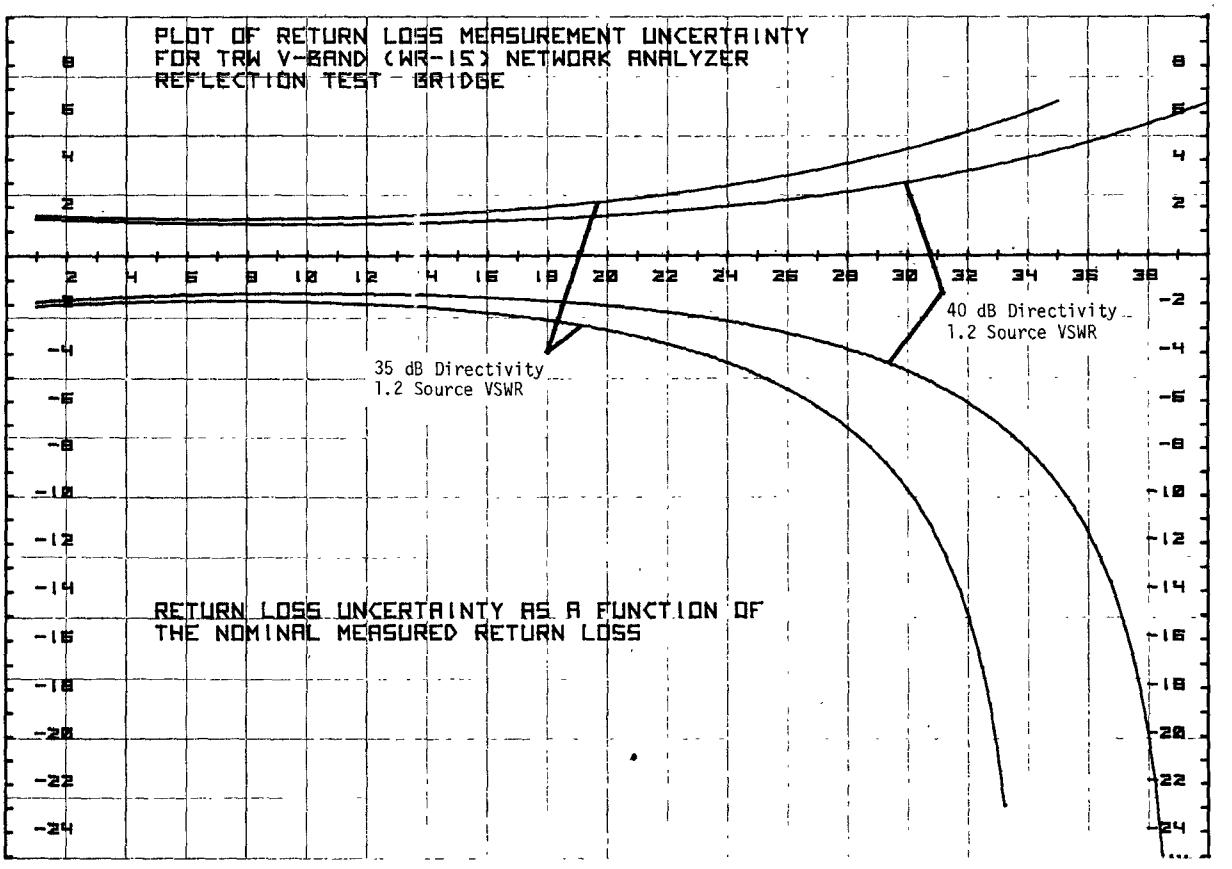

(a)

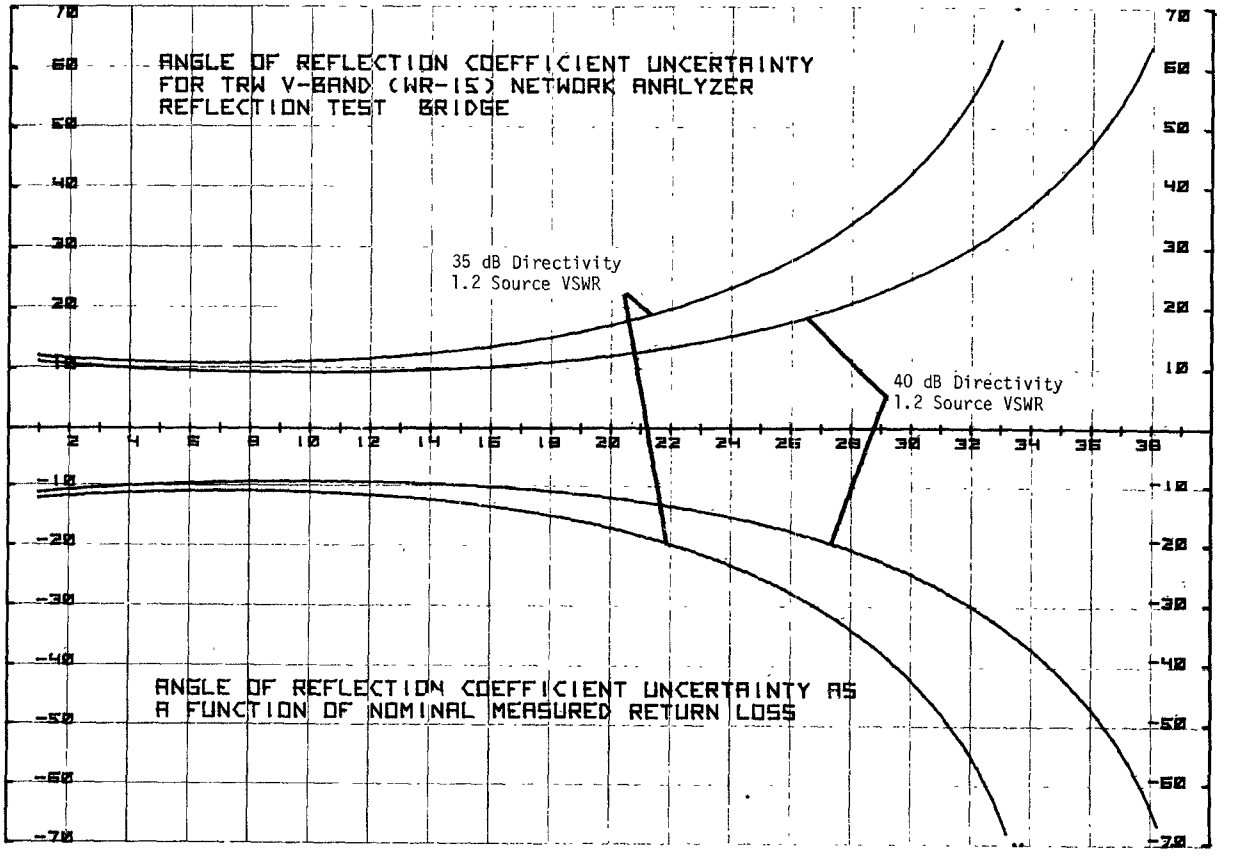

(b)

Fig. 5. Worst case uncertainties of the *V*-band reflection test unit. (a) Return loss uncertainty. (b) Phase uncertainty.

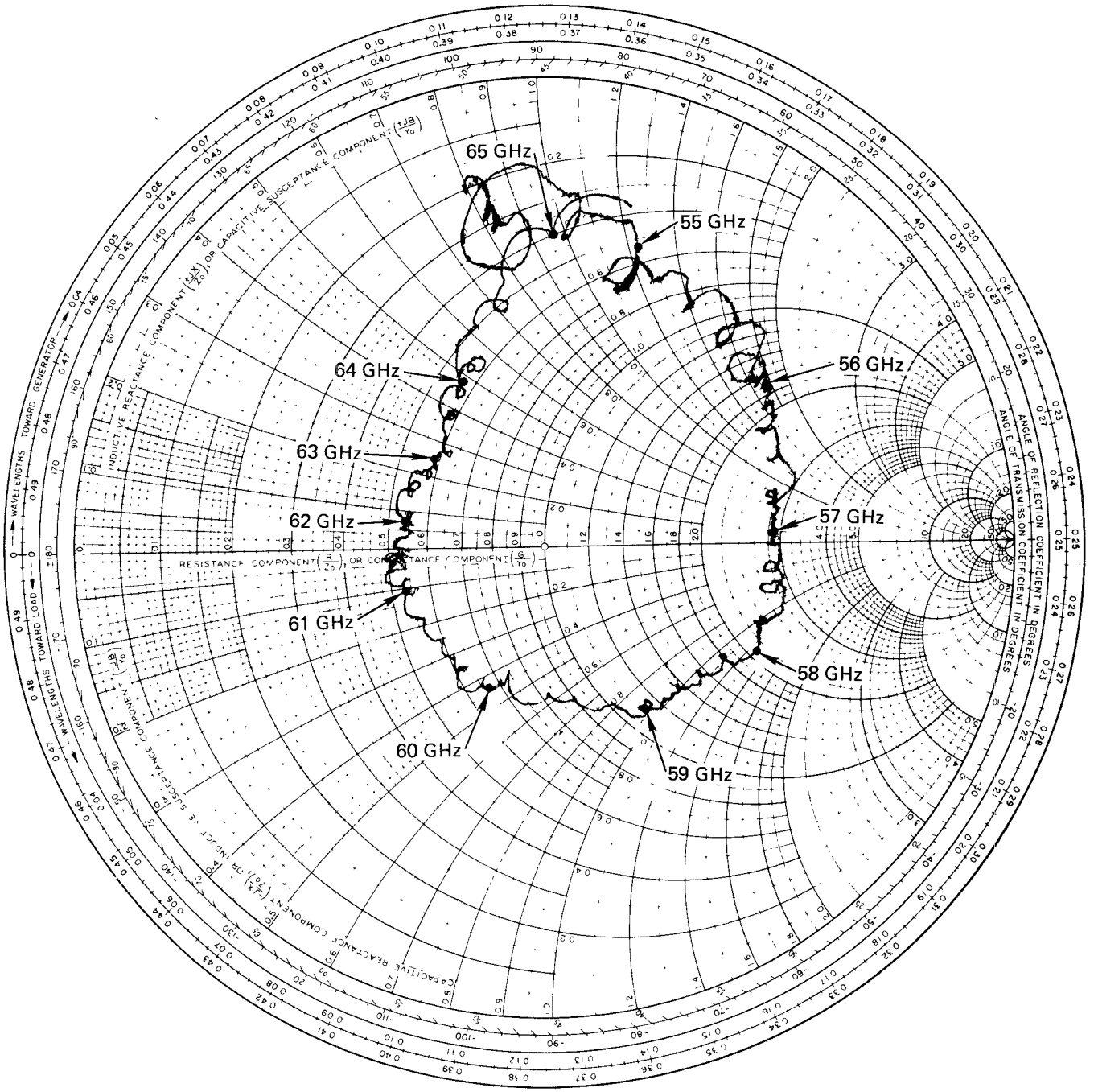

Fig. 6. RF impedance versus frequency of a single-ended mixer.

The directivity contributes greater error associated with the measurement of low values of the reflection coefficient, i.e., less than 0.2 which is a VSWR of 1.5:1. Similarly, source mismatch contributes greater error in the measurement of larger values of the reflection coefficient. Fig. 5(a) and (b) illustrates the calculated "worst case" uncertainties based on the measured worst case directivity of 35 dB and reflection coefficient of 0.09 of the V-band reflection test unit. As a comparison, magnitude and phase uncertainties are plotted for a commercial waveguide reflection test unit which has a directivity of 40 dB and source mismatch of 0.1.

Device Characterization

Two types of devices have been characterized by using the V-band network analyzer. One is a single-ended mixer designed for narrow-band operations at V-band frequencies. Fig. 6 shows the RF impedance plot on the Smith chart for the single-ended mixer measured by the V-band network analyzer over the frequency range from 55 to 65 GHz. The continuous display of the RF impedance covering the entire RF range with a single sweep clearly indicates the advantage of the broad-band characteristics of the design. In the RF impedance measurement for the single-ended mixer, no optimization of device performance or de-embedding of the device was performed. As for a comparison, the RF impedance of the mixer was also measured by using the slotted line techniques. The results, shown in Table I, demonstrate the excellent correlation between the two techniques, certainly within the uncertainty limits of the system established by the effective directivity of 35 dB and source reflection coefficient of 0.09. Fig. 7 shows an RF impedance plot on the Smith chart of an avalanche diode amplifier operating between 60.5 and 62 GHz. A maximum gain of approximately 3.3 dB at 70-mA

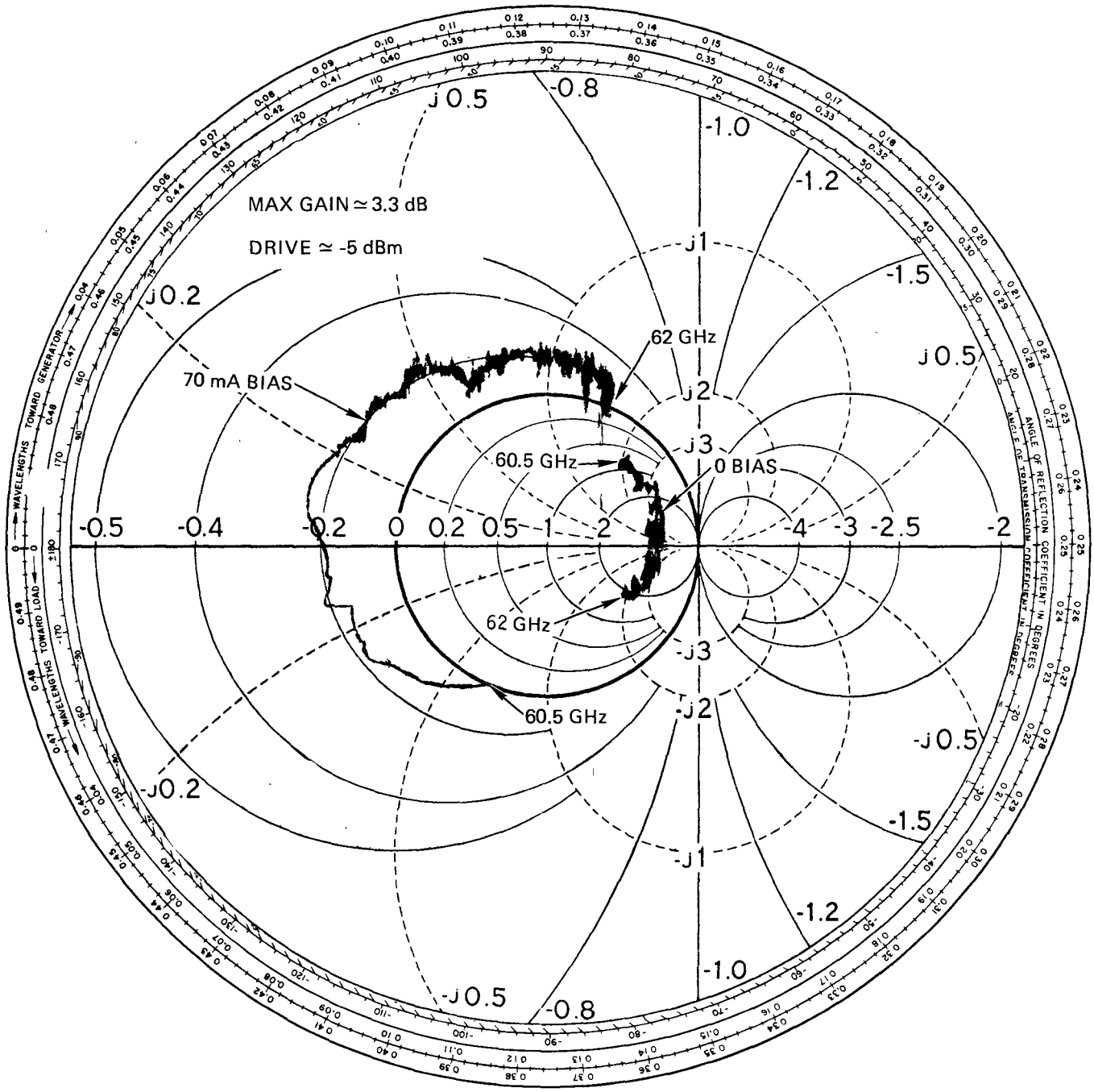

Fig. 7. RF impedance versus frequency of an avalanche diode amplifier.

TABLE I
SINGLE-ENDED MIXER VSWR MEASUREMENTS

Frequency (GHz)	Bias Current (mA)	VSWR Measured by Slotted Line	VSWR Measured by the Present Unit	Range of VSWR* Measured Uncertainty
55	0.370	5.2	5.0	3.32 - 8.85
56	0.528	3.4	3.7	2.73 - 5.33
57	0 668	2.7	2.9	2.31 - 3.92
58	0.746	3.0	3.0	2.36 - 3.94
59	0.898	2.15	2.3	1.94 - 2.77
60	0.875	1.85	1.95	1.70 - 2.25
61	0.804	1.77	1.9	1.67 - 2.17
62	0.868	1.79	1.85	1.66 - 2.10
63	0.946	2.0	1.9	1.67 - 2.17
64	0.868	2.4	2.3	1.94 - 2.77
65	0.587	5.8	5.0	3.32 - 8.85

* Calculated from (1) based on an effective directivity of 35 dB and source reflection coefficient of 0.09.

bias current was measured, which is in good agreement with results obtained by direct power measurements.

CONCLUSION

Overall system performance of the V-band network analyzer is encouraging, particularly the ultrabroad IF bandwidth which results in a continuous measurement covering a 10-GHz band with a single sweep. The key component responsible for the broad-band performance of the present design is a matched pair of broad-band mixers capable of operation over wide RF and IF bandwidths. The present design definitely is not limited to operate over the 55–65-GHz range. This range was selected primarily because it is the range covered by commercial sweepers presently available. Based on the same design principle, the operating frequency can be extended to other ranges by scaling.

References

[1] L. E. Dickens *et al.*, "A mixer and solid state LO for a 60 GHz receiver," *IEEE-GMTT International Microwave Symposium*, pp. 188–190, May 19, 1971.
[2] L. T. Yuan, "A low noise broadband *Ka*-band waveguide mixer," *IEEE-GMTT International Microwave Symposium*, pp. 272–273, May 12, 1975.
[3] A. L. Lance, "Evaluate couplers fast and accurately," *Microwaves*, vol. 9, pp. 34–36, Nov. 1970.
[4] P. C. Ely, Jr., "Swept frequency techniques," *Proc. IEEE*, vol. 55, pp. 991–1002, June 1967.
[5] Hewlett Packard Application Note 183, "High frequency swept measurements," Appendix B.

Discussion of a 2-Gap Waveguide Mount

ROBERT L. EISENHART, MEMBER, IEEE

***Abstract*—An equivalent circuit is presented for a commonly used waveguide diode mount, providing the means for accurate theoretical analysis and design of components previously considered possible only by empirical means. Several applications are discussed and experimental confirmation is included for a variety of circuit configurations.**

I. Introduction

The purpose of this short paper is to discuss an equivalent circuit for a waveguide mounting structure. This circuit has a great deal of flexibility in application, providing accurate description for a variety of circuit configurations.

Basically, the circuit was developed to describe the waveguide mount shown in Fig. 1 which we will call the 2-gap post mount. This circuit has been used as a varactor-tuned Gunn oscillator mount [1] but was not fully understood. In addition, there is a biasing difficulty because a wire must be connected to midpost with a minimum disturbance of the surrounding fields. Whether or not the understanding made available through this equivalent circuit proves the mount in Fig. 1 to be very useful is not the major interest here. Through parallel research effort, additional knowledge has been gained which, when used in conjunction with the 2-gap equivalent circuit, allows application to a much wider range of waveguide configurations. An equivalence has been established between a coaxial entry on the bottom of the waveguide and a gap in the post at the bottom [2]. An obvious extension of this idea is that shown in Fig. 2, where the 2-gap equivalent circuit can be applied to any one of the three configurations shown. The power of this analysis is more readily apparent now, since Fig. 2 (b) and (c) is very commonly used. Note also that there is no restriction on the loading of the coaxial line or the two waveguide arms. Fig. 2(b) could represent a parametric amplifier, upconverter, or downconverter which has the appropriate filter in the coax line and a varactor in the gap. It could also be an IMPATT or Gunn oscillator with a sliding short for tuning in the coax, or perhaps use the coax to model an imperfect bias. One of the most common applications of Fig. 2(c) is the oscillator circuit attributed to Kurokawa [3] which recesses an IMPATT diode in one coax arm and puts a matched load in the other. Typically, there is a sliding short on one waveguide arm with the other being the output. Examples of circuits from Fig. 2(b) and (c) will be discussed in the experimental results.

II. Equivalent Circuit Development

The 2-gap equivalent circuit is based upon an extension of the single-gap development which was published in August 1971 [4]. It is therefore necessary that, in order to fully understand and use the material presented here, the reader should be familiar with [4], a detailed review of which would be repetitious. The extension in concept and circuit analysis is relatively straightforward from the single to the double gap.

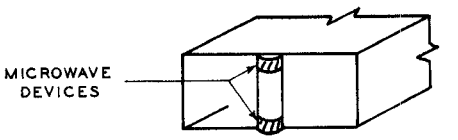

Fig. 1. 2-gap post mount.

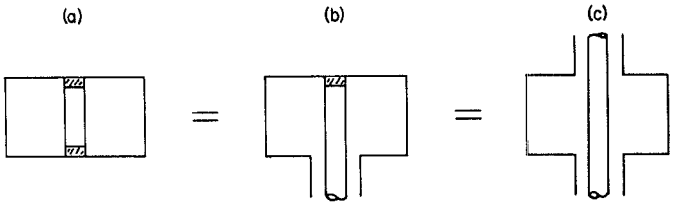

Fig. 2. Equivalent waveguide configurations for which the 2-gap circuit can be applied. (a) Double gap. (b) Gap/coax. (c) Double coax.

The concept behind the single-gap circuit is that each waveguide mode exists (a doubly infinite number) and has a loading effect on the gap driving point impedance Z_R. To accurately describe the characteristics of a particular mount configuration, it is necessary to determine the coupling mechanism between the gap terminals and each of these modes. This complex coupling action is best described by use of an equivalent circuit. Conceptually, then, the circuit only contains ideal coupling transformers between the gap and the modes, considering the mode effects as external loads. These modes are described in terms of a mode impedance which is dependent only upon the waveguide parameters and the mode indices. These mode impedances are

$$Z_H = j\frac{\eta b}{a(2-\delta_0)}\left(\frac{f}{\sqrt{f_c^2 - f^2}}\right)\left(\frac{(mb)^2}{(mb)^2 + (na)^2}\right) \tag{1a}$$

$$Z_E = -j\frac{\eta b}{a(2-\delta_0)}\left(\frac{\sqrt{f_c^2 - f^2}}{f}\right)\left(\frac{(na)^2}{(mb)^2 + (na)^2}\right) \tag{1b}$$

where

η free-space impedance = $120\pi\ \Omega$;
m,n mode indices with;
m field variation in the x direction;
n field variation in the y direction;
f_c mode cutoff frequency = $[(mc/2a)^2 + (\eta c/2b)^2]^{1/2}$;
c free-space velocity of propagation;

$$\delta_0 = \begin{cases} 1, & n = 0 \\ 0, & \text{otherwise.} \end{cases}$$

The waveguide dimensions a,b are defined in Fig. 3, along with the dimensional parameters associated with the two gaps and the post. These impedances happen to sum directly, resulting in what is called the mode pair impedance [4].

$$Z_{mn} = Z_H + Z_E. \tag{2}$$

The mode pair impedance will be resistive for propagating modes, reactive for evanescent modes, and is the terminating load at each mode port of the coupling circuit [4, fig. 5]. Fig. 4 shows this single-gap circuit but with the mode impedances combined for each value of n, where

$$Z_{Dn} = \sum_{m=1}^{M_1} Z_{mn}\kappa_{pm}^2, \qquad \text{for } n = 0,1,\cdots,N_1 \tag{3}$$

Manuscript received May 17, 1976; revised July 26, 1976.
The author is with Hughes Aircraft Company, Culver City, CA 90230.